Biochemical and Biophysical Research Communications 434 (2013) 252–257

Contents lists available at SciVerse ScienceDirect

Biochemical and Biophysical Research Communications

journal homepage: www.elsevier.com/locate/ybbrc

Optimal microscopic systems for long-term imaging of intracellular calcium using a ratiometric genetically-encoded calcium indicator

Akitoshi Miyamoto [a,b], Hiroko Bannai [a], Takayuki Michikawa [a,c,d], Katsuhiko Mikoshiba [a,e,*]

[a] Laboratory for Developmental Neurobiology, RIKEN Brain Science Institute, 2-1 Hirosawa, Wako, Saitama 351-0198, Japan
[b] Division of Neuronal Network, Department of Basic Medical Sciences, Institute of Medical Science, The University of Tokyo, Minato-ku, 4-6-1 Shirokanedai, Tokyo 108-8639, Japan
[c] Brain Science Institute, Saitama University, 255 Shimo-Okubo, Sakura-ku, Saitama 338-8570, Japan
[d] Laboratory for Behavioral Genetics, RIKEN Brain Science Institute, 2-1 Hirosawa, Wako, Saitama 351-0198, Japan
[e] Calcium Oscillation Project, International Cooperative Research Project and Solution-Oriented Research for Science and Technology, Japan Science and Technology Agency, 4-1-8 Honmach Kawaguchi, Saitama 332-0012, Japan

ARTICLE INFO

Article history:
Received 13 February 2013
Available online 25 March 2013

Keywords:
Genetically encoded Ca^{2+} indicators
Illumination power
Ca^{2+} oscillation
Wide-field fluorescent microscope
Multipoint scanning confocal system
Single-point scanning confocal system

ABSTRACT

Monitoring the pattern of intracellular Ca^{2+} signals that control many diverse cellular processes is essential for understanding regulatory mechanisms of cellular functions. Various genetically encoded Ca^{2+} indicators (GECIs) are used for monitoring intracellular Ca^{2+} changes under several types of microscope systems. However, it has not yet been explored which microscopic system is ideal for long-term imaging of the spatiotemporal patterns of Ca^{2+} signals using GECIs. We here compared the Ca^{2+} signals reported by a fluorescence resonance energy transfer (FRET)-based ratiometric GECI, yellow cameleon 3.60 (YC3.60), stably expressed in DT40 B lymphocytes, using three different imaging systems. These systems included a wide-field fluorescent microscope, a multipoint scanning confocal system, and a single-point scanning confocal system. The degree of photobleaching and the signal-to-noise ratio of YC3.60 in DT40 cells were highly dependent on the fluorescence excitation method, although the total illumination energy was maintained at a constant level within each of the imaging systems. More strikingly, the Ca^{2+} responses evoked by B-cell antigen receptor stimulation in YC3.60-expressing DT40 cells were different among the imaging systems, and markedly affected by the illumination power used. Our results suggest that optimization of the imaging system, including illumination and acquisition conditions, is crucial for accurate visualization of intracellular Ca^{2+} signals.

1. Introduction

Ca^{2+} acts as an intracellular messenger, relaying information that regulates the activity of proteins involved in many critical processes of life and death. To control these diverse cellular processes, intracellular Ca^{2+} signals have evolved to be highly versatile in terms of the amplitude, frequency, and duration of the Ca^{2+} transient [1]. Extracellular stimuli induce Ca^{2+} signals with unique spatiotemporal patterns to trigger appropriate cellular responses, such as cellular motility [2], exocytosis of cytolytic granules [3], transcription factor activation [4–7], and cell fate decisions [8,9]. Visualizing precise patterns of Ca^{2+} signals is essential for understanding the mechanisms regulating these cellular functions. For this purpose, various tools such as chemical Ca^{2+} indicators [10] and genetically encoded Ca^{2+} indicators (GECIs) [11–13] have been developed for Ca^{2+} imaging. These tools allow monitoring of Ca^{2+} dynamics in living cells by fluorescence microscopy. Progresses in GECIs in recent 15 years enabled Ca^{2+} imaging studies that were difficult with chemical Ca^{2+} indicators, for example, long-term stable Ca^{2+} measurements in specific cell types or local subcellular domains, and GECIs are now inevitable tools for Ca^{2+} imaging both *in vitro* and *in vivo*. Among GECIs, one of the most widely-used GECI family is a yellow cameleon [11,12], which is the fluorescence resonance energy transfer (FRET)-based ratiometric GECIs permitting quantitative Ca^{2+} imaging that can eliminate artifacts caused by indicator concentration and cell thickness or movement.

As the demand for imaging of dynamic cellular processes has increased, several types of imaging systems including the wide-field fluorescent microscope (WFM) and confocal systems [14] have also been developed further. Multiple options for fluorescence microscopy illumination and image detection are now available in each imaging system. For instance, a mercury lamp, a Xenon lamp, and a light-emitting diode (LED) could be used for fluorescence excitation, while a conventional cooled charge-coupled device

* Corresponding author at: Laboratory for Developmental Neurobiology, RIKEN Brain Science Institute, 2-1 Hirosawa, Wako, Saitama 351-0198, Japan. Fax: +81 48 467 9744.
E-mail address: mikosiba@brain.riken.jp (K. Mikoshiba).

0006-291X/$ - see front matter © 2013 Elsevier Inc. All rights reserved.
http://dx.doi.org/10.1016/j.bbrc.2013.02.112

(CCD) camera, an electron multiplying CCD (EM-CCD) camera, and a camera with a complementary metal oxide semiconductor (CMOS) image sensor are available as detectors in WFM systems. Several options are also available for optical sectioning in confocal microscopy, such as single-point scanning method using photomultiplier tubes (PMTs) [14] and multipoint scanning method [15], in which a cooled CCD camera, an EM-CCD camera or a CMOS image sensor is also used as detector.

The diversities of imaging systems raise the question as to which system is ideal for long-term Ca^{2+} imaging using GECIs. In this study, we compared the fluorescence signal of yellow cameleon 3.60 (YC3.60) [12] as detected by three different imaging systems. These systems included WFM, a multipoint scanning confocal system (MPSC), and a single-point scanning confocal system (SPSC). We here report that B-cell antigen receptor (BCR)-mediated Ca^{2+} mobilization in DT40 cells was strikingly affected by illumination power and imaging systems used, and that SPSC equipped with a beam splitter was the most suitable imaging system for monitoring Ca^{2+} signals with YC3.60 among the imaging systems tested.

2. Materials and methods

2.1. Cell preparation

Stable cell lines expressing YC3.60 were established from DT40 cells as described previously [16] using the plasmid (pcDNA3; Invitrogen) encoding YC3.60 [12] (a gift from T. Nagai and A. Miyawaki).

2.2. Imaging

Enhanced cyan fluorescent protein (ECFP) and Venus [17] signals from YC3.60 were acquired every 5 s for 30 min using WFM, MPSC, and SPSC (for detail microscope configurations, see Supplementary Materials). Illumination powers were measured using an excitation light irradiance meter developed by RIKEN BSI–Olympus Collaboration Center (BOCC) (for detail, see http://rikenbocc.brain.riken.jp/BOCC_technological_innovation_e.html and http://rikenbocc.brain.riken.jp/files/ExcitationLightIrradianceMeter_Eng_001.pdf).

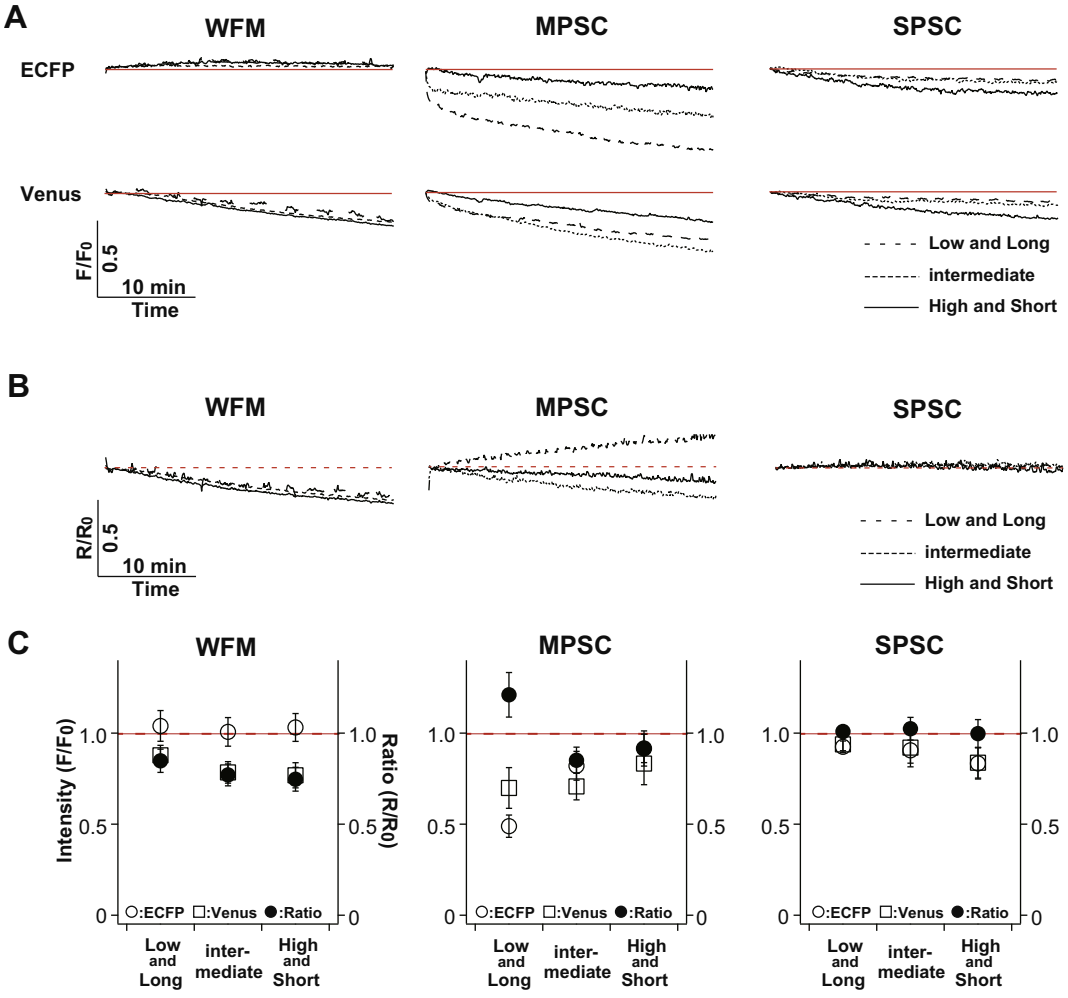

Fig. 1. Fluorescence excitation conditions affect the degree of photobleaching. (A) Changes in the ECFP (top) and Venus (bottom) fluorescence intensities of YC3.60 (F/F_0). Mean F/F_0 values of 36–60 measurements were plotted against time. Red lines represent F_0. Low and Long, Intermediate, and High and Short represent illumination conditions with exposure for a long period under low illumination power, an intermediate period under intermediate illumination power, and a short period under high illumination power, respectively (for detail, see Supplementary Table S2). (B) The ratio change of YC3.60 (Venus/ECFP) calculated from the data shown in (A). Red broken lines represent R_0. (C) The fluorescence intensity (F/F_0) of ECFP (open circle) and Venus (open square) and the ECFP/Venus ratio (R/R_0, closed circle) of YC3.60 signals 30 min after the onset of recording. Red broken lines represent F_0 and R_0. Bars represent standard deviation (SD). (For interpretation of the references to color in this figure legend, the reader is referred to the web version of this article.)

2.3. Statistical analysis

Statistical analyses were performed using one-way analysis of variance (ANOVA) followed by a post hoc comparison using the Tukey–Kramer multiple comparison procedure. Student's *t*-test was used for the comparison between two groups. Pearson's correlation test was used for the measurement of the strength of a relationship between two variables.

3. Results and discussion

3.1. Illumination method affects the degree of photobleaching and signal-to-noise ratio of YC3.60

As recent advances in microscopes and detectors have broadened choice of imaging systems to observe dynamic Ca^{2+} signals in living cell, it is essential to understand detailed properties of GECIs under different imaging systems. For this purpose, we compared the spatiotemporal patterns of Ca^{2+} signals reported by YC3.60 among three different imaging systems, WFM, MPSC, and SPSC (see Supplementary Materials and Methods, Table S1). DT40, an avian leukosis virus-induced chicken pre-B-cell line [18], stably expressing a GECI protein YC3.60 was used in this study to avoid complication posed by a large cell-to-cell variation in the Ca^{2+} indicator concentration by transient expression.

First, to determine the optimal condition for fluorescence imaging, the degree of photobleaching during the 30 min-recording period and the S/N ratio of YC3.60 were examined using each imaging system. The illumination power and exposure time were modified so that the total excitation energy, which was the product of the illumination power and exposure time, was kept essentially constant for each imaging system (Supplementary Table S2). Thus, the following three different conditions were tested: high illumination power for a short period (high and short), low illumination power for a long period (low and long), or intermediate illumination power for an intermediate period (intermediate). All the illumination conditions allowed the recording of signals with sufficient spatial resolution (Supplementary Fig. S1).

Fig. 1A and B shows the ECFP and Venus fluorescence intensities by the excitation of ECFP and Venus/ECFP emission ratio of YC3.60 measured in DT40 cells plotted against time, respectively. Fluorescence signals were acquired at 0.2 Hz for 30 min. In all three imaging systems, the ECFP and Venus fluorescence intensities almost gradually decreased during imaging in the absence of any stimulation. However, the degree of photobleaching of each fluorescent protein signal 30 min after the onset of recording was dependent on the excitation conditions and imaging system (Fig. 1A and C). With WFM, the low and long condition resulted in the least bleaching of fluorescence signals of YC3.60. With MPSC, the least bleaching of fluorescence signals were induced by excitation under the high and short condition. With SPSC, the degree of photobleaching under the low and long and intermediate conditions were less than that under the high and short condition (Fig. 1C).

These differences in the degrees of photobleaching of the ECFP and Venus fluorescence signals affected the Venus/ECFP emission ratio of the YC3.60 signal, which is an indication of the intracellular Ca^{2+} concentration (Fig. 1B). Considering that no stimulation inducing Ca^{2+} mobilization was applied during the recording time, the normalized Venus/ECFP emission ratio (R/R_0) was expected to be 1. However, with WFM, the ratio actually decreased to 0.75 ± 0.07, 0.77 ± 0.06, and 0.84 ± 0.06 (58–60 cells) under the high and short, intermediate, and low and long conditions, respectively, because of photobleaching of the Venus fluorescence signals during the 30-min recording period. With MPSC, the ratio decreased to 0.85 ± 0.07 and 0.91 ± 0.08 (36 and 42 cells) under the intermediate and high and short conditions, respectively, whereas

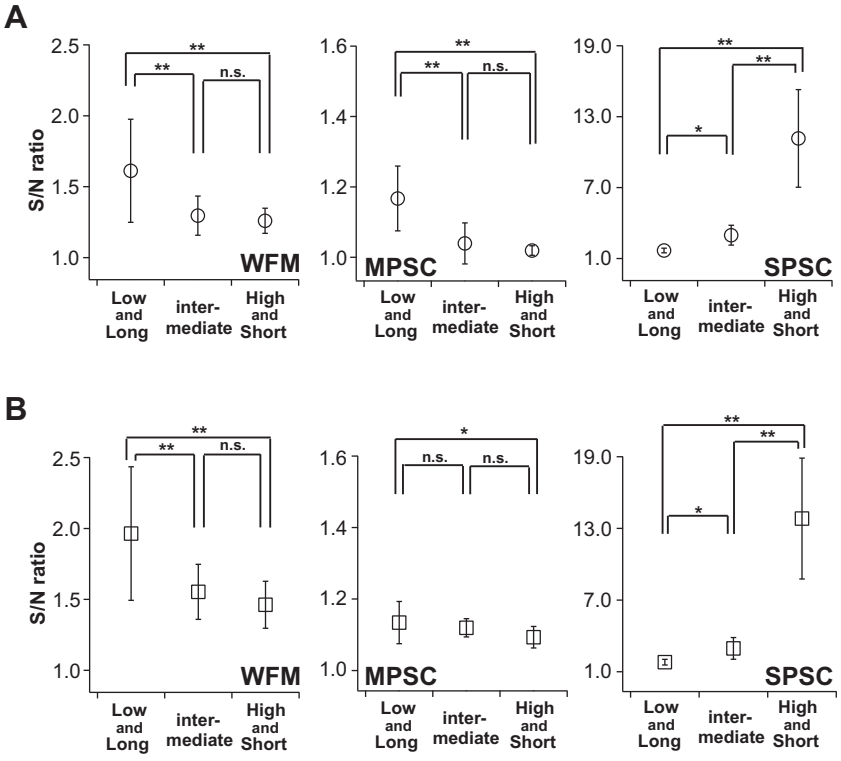

Fig. 2. Illumination affects the signal-to-noise (S/N) ratio. The S/N ratio of ECFP (A) and Venus (B) under different illumination conditions. Signal and noise indicate the fluorescence intensity in YC3.60-expressing DT40 cells and that in the background, respectively. S/N ratios were calculated from the mean value of the first 2 min of imaging (n = 36–60). Bars represent SD. $^{*}p < 0.05$, $^{**}p < 0.01$, n.s.: not significant, Tukey–Kramer test.

the ratio increased to 1.21 ± 0.12 (40 cells) under the low and long condition. With SPSC, the Venus/ECFP ratio of the YC3.60 signals remained virtually constant and approached 1 [low and long: 1.01 ± 0.03; intermediate: 1.02 ± 0.06; high and short: 1.00 ± 0.08; (50–52 cells)] (Fig. 1B and C).

The S/N ratio (see Supplementary Material and Methods) of the ECFP and Venus fluorescence intensities was also affected by the illumination conditions (Fig. 2A and B, respectively. For still images, see Supplementary Fig. S1). With WFM and MPSC, the low and long condition resulted in a higher S/N ratio than the high and short and intermediate conditions. The S/N ratio with SPSC was higher than that with other imaging systems; the S/N ratio was significantly improved by an increase in the illumination power and reached 13.8 ± 5.1 under the high and short condition.

Considering the effect on the degree of photobleaching and the S/N ratio, we determined the optimal illumination condition for each imaging system. Exposure for a long period under low illumination power (150 ms × 295 μW) was optimal for WFM and that for a short period under high illumination power (100 ms × 60 μW) was best for MPSC. The intermediate imaging condition (1 frame per second × 30 μW) was most ideal for SPSC.

3.2. Stimulation-induced Ca^{2+} signals are dependent on illumination powers and imaging systems

BCR stimulation induces a rapid increase in cytoplasmic free Ca^{2+} concentration due to Ca^{2+} release from the intracellular stores [19] and Ca^{2+} influx from the extracellular environment in DT40 cells [20]. Therefore, we further compared the BCR stimulation-evoked Ca^{2+} signals reported by YC3.60 using the three imaging systems under the optimal illumination condition for each system. BCRs on the surface were stimulated with 2 μg/ml anti-chicken IgM antibody (M4) [21], and YC3.60 signals were detected using WFM, MPSC, and SPSC. As reported by previous studies using a chemical Ca^{2+} dye, Fura-2, and WFM equipped with a Xenon lamp [22,23], M4 stimuli evoked a biphasic Ca^{2+} signaling response in DT40 cells expressing YC3.60; the first component was the initial large Ca^{2+} spike at the onset of M4 application and the second was repetitive Ca^{2+} transients lasting for at least 10 min (Ca^{2+} oscillation) following the initial large Ca^{2+} spikes, both of which were detected under WFM, MPSC, and SPSC (Fig. 3A and B). The initial large Ca^{2+} spike in response to BCR stimulation were observed in 100% of DT40 cells using all imaging systems (Supplementary Fig. S2). However the percentage of cells that showed Ca^{2+} oscillation was remarkably less when observed under WFM (37.8 ± 8.9%)

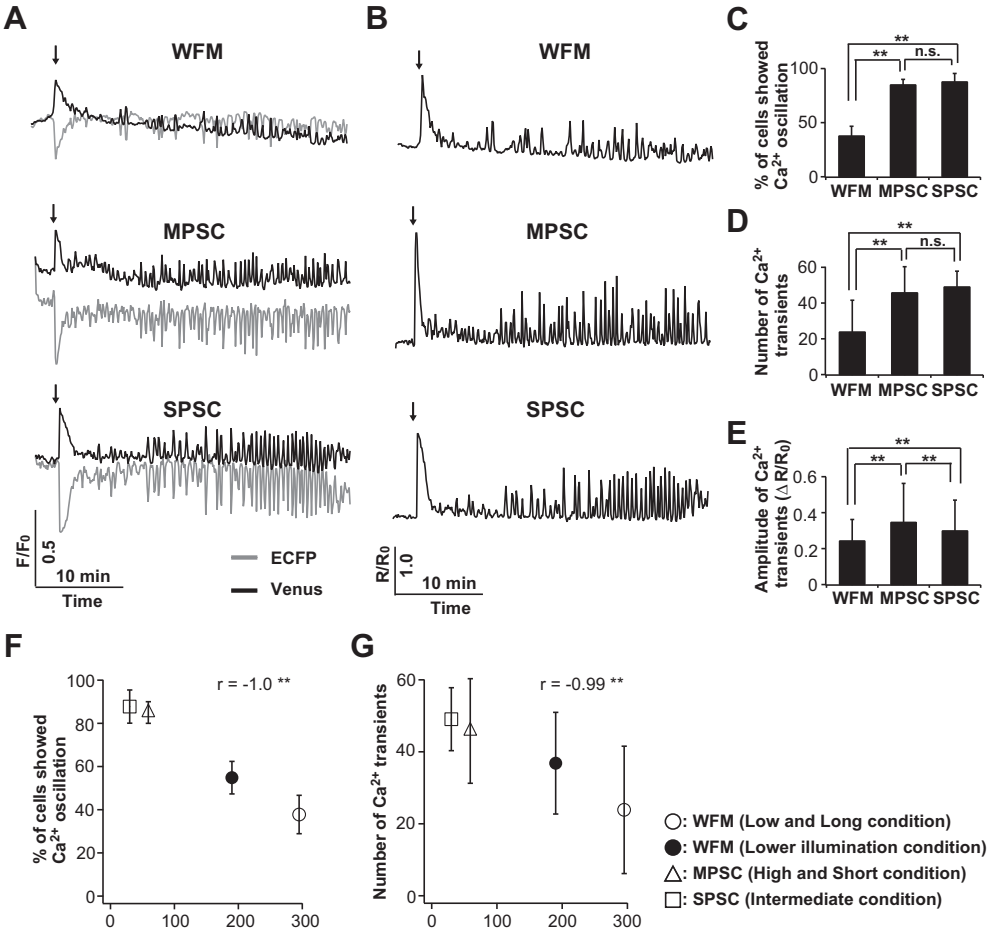

Fig. 3. BCR stimulation-evoked Ca^{2+} signals are dependent on the imaging system. (A) Changes in the fluorescence signals acquired from a single YC3.60-expressing DT40 cell. The onset of M4 stimulation (2 μg/ml) is shown by the arrow. (B) The change in the Venus/ECFP emission ratio of YC3.60 (Venus/ECFP) calculated from the data shown in (A). (C) The percentage of cells showing Ca^{2+} oscillations lasting for at least 10 min following a BCR stimulation-evoked Ca^{2+} spike ($n = 3$ cultures). (D) The number of Ca^{2+} transients during Ca^{2+} oscillations ($n = 53$–64 cells). (E) Peak amplitude of Ca^{2+} spikes during Ca^{2+} oscillations ($n = 53$–64 cells). Value and bars represent mean and SD, respetively. $^{**}p < 0.01$; n.s.: not significant, Tukey–Kramer test for (C–E). (F and G) The percentage of the cells that showed Ca^{2+} oscillation (F), and the number of Ca^{2+} transients during Ca^{2+} oscillation (G), plotted against the illumination powers. Bars represent SD. $^{**}p < 0.01$, Pearson's correlation test for (F and G).

than under MPSC and SPSC (approximately 85%) (Fig. 3C); the former was comparable to the approximate 30% value reported in a previous study [22]. In addition, the number (Fig. 3D) and amplitude (Fig. 3E) of Ca^{2+} transients during Ca^{2+} oscillation were reduced when observed using WFM than using MPSC and SPSC.

The excitation light illumination during fluorescence live cell imaging induces phototoxicity in cells at higher doses [24,25]. The illumination power used in WFM was markedly higher than that used in MPSC and SPSC (Supplementary Table S2); this could affect the observed Ca^{2+} signals through reaction with YC3.60 or endogenous biomolecules. To investigate this possibility, we set a new imaging condition using WFM by reducing the illumination power and exposure time to as low and as short as possible and increasing binning of the CCD camera (lower illumination condition; for detail, see Supplementary Table S3). Under this condition, in addition to loss of spatial resolution (Supplementary Fig. S1), the S/N ratio of the ECFP and Venus fluorescence intensities were markedly decreased to 1.22 ± 0.06 and 1.50 ± 0.13 (58 cells), respectively. However, the photobleaching of the ECFP and Venus fluorescence signals during the 30-min recording period were almost suppressed (F/F_0: 0.94 ± 0.07 for ECFP and 0.98 ± 0.06 for Venus; Supplementary Fig. S3A and S3B). Indeed, the degree of photobleaching of the Venus fluorescence signals was less than that observed with WFM, MPSC, and SPSC ($p < 0.01$, Tukey–Kramer test). We then compared the BCR stimulation-evoked Ca^{2+} signals under the lower illumination condition (Supplementary Fig. S3C and S3D) with that using WFM, MPSC, and SPSC (Fig. 3A). The percentage of cells that showed Ca^{2+} oscillation after Ca^{2+} spikes (Supplementary Fig. S3E) and the number of Ca^{2+} transients during Ca^{2+} oscillation (Supplementary Fig. S3F) under the lower illumination condition were significantly greater than those using WFM but less than those using MPSC and SPSC, irrespective of the reduced degree of photobleaching under the lower illumination condition (Supplementary Fig. S3B). Surprisingly, the percentage of cells that showed Ca^{2+} oscillation after Ca^{2+} spikes (Supplementary Fig. S3G) and the number of Ca^{2+} transients during Ca^{2+} oscillation (Supplementary Fig. S3H) did not correlate with the degree of photobleaching after 30 min recording period (correlation coefficients: $r = -0.24$ and -0.03, respectively), suggesting that the reduced Ca^{2+} oscillation is not due to artifacts induced by the photobleach of YC3.60. Instead, the illumination power used negatively correlated with the percentage of cells that showed Ca^{2+} oscillation and with the number of Ca^{2+} transients (Fig. 3F and G; correlation coefficients: $r = -1.0$ and -0.99, respectively), regardless of the imaging system used. These results indicate that Ca^{2+} reactivity in DT40 cells is sensitive to the excitation light illumination power.

It is also possible that the exposure time and the inherent difference in illumination methods could also affect the degree of phototoxicity. Indeed, the exposure time was markedly longer for WFM than for the confocal systems: the cells were uniformly illuminated for 60 ms to obtain an adequate S/N ratio under the WFM condition. In contrast under SPSC, the illumination duration at each point (pixel dwell time) was estimated to be 4.5 μs for the intermediate condition. Considering that only 4% of the Nipkow disk in CSU-X1 is perforated with pinholes [15,26], the actual exposure time at each point in MPSC is estimated to be 4 ms [27], although the exposure time was set to 100 ms. WFM has been widely used in Ca^{2+} imaging studies. However, considering that WFM intrinsically has more potential for inducing phototoxicity than confocal systems as discussed above, more effort to reduce the excitation energy and increase the S/N ratio would be required to accurately visualize intact Ca^{2+} signals using this system. The use of a sensitive detector such as an EM-CCD camera, which allows acquisition of faint fluorescence signals at better S/N ratios, would be effective in reducing the exposure time and illumination dose. Even with confocal systems, technical advances to reduce illumination power with improved S/N ratios would lead to better understanding of real Ca^{2+} signals in living cells [28].

Ca^{2+} oscillation detected using MPSC and SPSC showed equivalent numbers of Ca^{2+} transients during Ca^{2+} oscillation (Fig. 3D). SPSC was equipped with a beam splitter; thus the ECFP and Venus signals were obtained simultaneously. In contrast, MPSC relied on a filter exchanger, and therefore, there was a slight lag between the acquisition of the ECFP and Venus signals (655 ± 1 ms for the high and short condition, Supplementary Fig. S4). Because YC3.60 was a FRET-based GECI, the decrease in the ECFP fluorescence intensity and the increase in the Venus fluorescence intensity correlated with an increase in cytoplasmic free Ca^{2+} [11], i.e., the changes in the ECFP and Venus fluorescence intensities should theoretically show symmetric responses. However, when observed at higher time resolution, several asymmetric changes in ECFP and Venus fluorescence were observed (4 ± 2.3 events/30 min, 15 recordings) using MPSC (Fig. 4A, arrow). On the other hand, in all 15 experiments with SPSC, all ECFP and Venus spikes showed a symmetric response (Fig. 4B). The above data suggested that the observed time lag of 655 ± 1 ms between the acquisition of the ECFP and Venus signals using MPSC impaired observation of the temporal patterns of a Ca^{2+} transient, which is in the order of 30 s (Fig. 4). Therefore, when a ratiometric indicator is used for monitoring Ca^{2+} events with a high frequency, it is crucial to prevent time lags between acquiring signals at two wavelengths in order to obtain an accurate temporal pattern of Ca^{2+} signals.

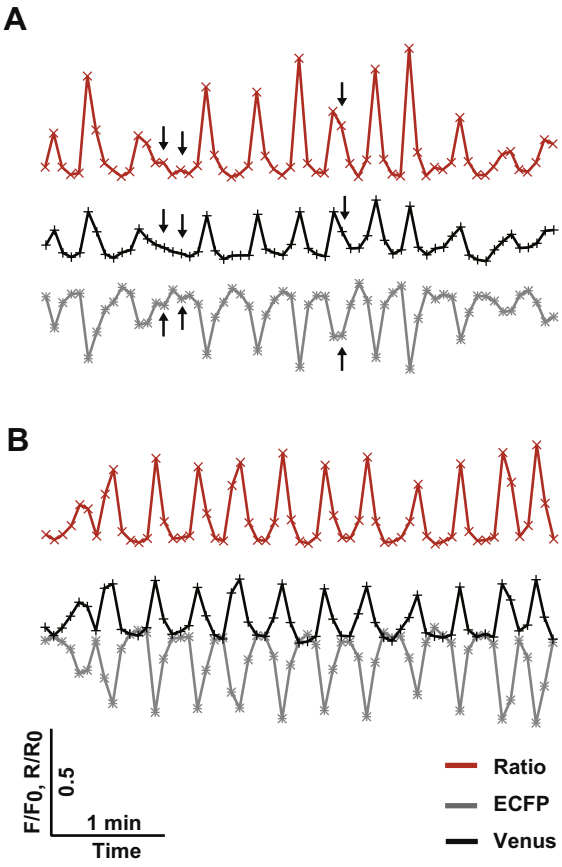

Fig. 4. High time resolution analysis of the ECFP (gray) and Venus (black) fluorescence intensities and the Venus/ECFP ratio of YC3.60 (red) during BCR stimulation-evoked Ca^{2+} oscillation. Examples of F/F_0 and R/R_0 recorded using MPSC (A) and those recorded using SPSC (B). Note that the changes in the ECFP and Venus fluorescence intensities showed asymmetric responses (arrows) with MPSC but not with SPSC.

Our results conclude that both illumination and acquisition conditions used for imaging systems can markedly affect the observed spatiotemporal patterns of Ca^{2+} signals and the observed shape of Ca^{2+} transients, in DT40 cells. At least under the conditions used in this study, SPSC equipped with a beam splitter was the most suitable system for cellular imaging using ratiometric indicators, because this system allowed simultaneous detection of the ECFP and Venus signals and could record signals with the highest S/N ratio and the lowest illumination power among the three imaging systems tested. Another benefit of using SPSC was the versatility of the pinhole size. In this study, we set the pinhole size of SPSC to the maximum (256 μm, 8 AU), which enabled us to collect the signal both inside and outside of the focal plane. In this manner, SPSC could function as a "WFM" rather than as a confocal microscope [29]. As a result, the SPSC settings described here enabled us to markedly reduce the exposure times and illumination power with a high S/N ratio compared with WFM and MPSC, and we considered it to report Ca^{2+} signals the most accurately among the three imaging systems. Therefore, SPSC used as WFM would be a powerful tool in future Ca^{2+} imaging studies, at least for the visualization of Ca^{2+} signals in DT40 cells. However, for Ca^{2+} imaging that requires recording at higher time resolution, e.g., recording the local Ca^{2+} signals that are known as Ca^{2+} puffs [1], MPSC with a beam splitter would be more suitable. This is because the EM-CCD camera can facilitate higher frequency recording.

In summary, our present study suggests the possibility that Ca^{2+} signals detected by unsuitable imaging systems do not report Ca^{2+} signals in living cells accurately, and this can impede our understanding of the regulatory mechanisms of cellular processes. Therefore, to better understand Ca^{2+} signals in cellular processes, more attention has to be paid to the selection and settings of the imaging systems used for Ca^{2+} imaging.

Acknowledgments

We thank Dr. T. Nagai and A. Miyawaki for YC3.60. We thank Nikon Instruments Inc. and T. Tajima and staffs of RIKEN BSI-Olympus Collaboration Center (BOCC) for technical support. This work was supported by grants from the Ministry of Education, Culture, Sports, Science and Technology of Japan (20220007 to K.M. and 24500476 to T.M.).

Appendix A. Supplementary data

Supplementary data associated with this article can be found, in the online version, at http://dx.doi.org/10.1016/j.bbrc.2013.02.112.

References

[1] M.J. Berridge, P. Lipp, M.D. Bootman, The versatility and universality of calcium signalling, Nat. Rev. Mol. Cell Biol. 1 (2000) 11–21.
[2] N.R. Bhakta, D.Y. Oh, R.S. Lewis, Calcium oscillations regulate thymocyte motility during positive selection in the three-dimensional thymic environment, Nat. Immunol. 6 (2005) 143–151.
[3] T.A. Lyubchenko, G.A. Wurth, A. Zweifach, Role of calcium influx in cytotoxic T lymphocyte lytic granule exocytosis during target cell killing, Immunity 15 (2001) 847–859.
[4] R.E. Dolmetsch, R.S. Lewis, C.C. Goodnow, J.I. Healy, Differential activation of transcription factors induced by Ca^{2+} response amplitude and duration, Nature 386 (1997) 855–858.
[5] R.E. Dolmetsch, K. Xu, R.S. Lewis, Calcium oscillations increase the efficiency and specificity of gene expression, Nature 392 (1998) 933–936.
[6] W. Li, J. Llopis, M. Whitney, G. Zlokarnik, R.Y. Tsien, Cell-permeant caged $InsP_3$ ester shows that Ca^{2+} spike frequency can optimize gene expression, Nature 392 (1998) 936–941.
[7] S. Feske, J. Giltnane, R. Dolmetsch, L.M. Staudt, A. Rao, Gene regulation mediated by calcium signals in T lymphocytes, Nat. Immunol. 2 (2001) 316–324.
[8] S. Feske, ORAI1 and STIM1 deficiency in human and mice: roles of store-operated Ca^{2+} entry in the immune system and beyond, Immunol. Rev. 231 (2009) 189–209.
[9] B. Qu, D. Al-Ansary, C. Kummerow, M. Hoth, E.C. Schwarz, ORAI-mediated calcium influx in T cell proliferation, apoptosis and tolerance, Cell Calcium 50 (2011) 261–269.
[10] G. Grynkiewicz, M. Poenie, R.Y. Tsien, A new generation of Ca^{2+} indicators with greatly improved fluorescence properties, J. Biol. Chem. 260 (1985) 3440–3450.
[11] A. Miyawaki, J. Llopis, R. Heim, J.M. McCaffery, J.A. Adams, M. Ikura, R.Y. Tsien, Fluorescent indicators for Ca^{2+} based on green fluorescent proteins and calmodulin, Nature 388 (1997) 882–887.
[12] T. Nagai, S. Yamada, T. Tominaga, M. Ichikawa, A. Miyawaki, Expanded dynamic range of fluorescent indicators for Ca^{2+} by circularly permuted yellow fluorescent proteins, Proc. Natl. Acad. Sci. USA 101 (2004) 10554–10559.
[13] K. Horikawa, Y. Yamada, T. Matsuda, K. Kobayashi, M. Hashimoto, T. Matsuura, A. Miyawaki, T. Michikawa, K. Mikoshiba, T. Nagai, Spontaneous network activity visualized by ultrasensitive Ca^{2+} indicators, yellow Cameleon-Nano, Nat. Methods 7 (2010) 729–732.
[14] J.G. White, W.B. Amos, M. Fordham, An evaluation of confocal versus conventional imaging of biological structures by fluorescence light microscopy, J. Cell Biol. 105 (1987) 41–48.
[15] S. Inoue, T. Inoue, Direct-view high-speed confocal scanner: the CSU-10, Methods Cell Biol. 70 (2002) 87–127.
[16] H. Sugawara, M. Kurosaki, M. Takata, T. Kurosaki, Genetic evidence for involvement of type 1, type 2 and type 3 inositol 1,4,5-trisphosphate receptors in signal transduction through the B-cell antigen receptor, EMBO J. 16 (1997) 3078–3088.
[17] T. Nagai, K. Ibata, E.S. Park, M. Kubota, K. Mikoshiba, A. Miyawaki, A variant of yellow fluorescent protein with fast and efficient maturation for cell-biological applications, Nat. Biotechnol. 20 (2002) 87–90.
[18] S. Kim, E.H. Humphries, L. Tjoelker, L. Carlson, C.B. Thompson, Ongoing diversification of the rearranged immunoglobulin light-chain gene in a bursal lymphoma cell line, Mol. Cell Biol. 10 (1990) 3224–3231.
[19] K. Mikoshiba, IP_3 receptor/Ca^{2+} channel: from discovery to new signaling concepts, J. Neurochem. 102 (2007) 1426–1446.
[20] E.M. Gallo, K. Cante-Barrett, G.R. Crabtree, Lymphocyte calcium signaling from membrane to nucleus, Nat. Immunol. 7 (2006) 25–32.
[21] C.L. Chen, J.E. Lehmeyer, M.D. Cooper, Evidence for an IgD homologue on chicken lymphocytes, J. Immunol. 129 (1982) 2580–2585.
[22] E.F. Eckenrode, J. Yang, G.V. Velmurugan, J.K. Foskett, C. White, Apoptosis protection by Mcl-1 and Bcl-2 modulation of inositol 1,4,5-trisphosphate receptor-dependent Ca^{2+} signaling, J. Biol. Chem. 285 (2010) 13678–13684.
[23] C. Li, X. Wang, H. Vais, C.B. Thompson, J.K. Foskett, C. White, Apoptosis regulation by Bcl-xL modulation of mammalian inositol 1,4,5-trisphosphate receptor channel isoform gating, Proc. Natl. Acad. Sci. USA 104 (2007) 12565–12570.
[24] R. Dixit, R. Cyr, Cell damage and reactive oxygen species production induced by fluorescence microscopy: effect on mitosis and guidelines for non-invasive fluorescence microscopy, Plant J. 36 (2003) 280–290.
[25] M.B. Vrouenraets, G.W. Visser, G.B. Snow, G.A. van Dongen, Basic principles, applications in oncology and improved selectivity of photodynamic therapy, Anticancer Res. 23 (2003) 505–522.
[26] P.S. Maddox, B. Moree, J.C. Canman, E.D. Salmon, Spinning disk confocal microscope system for rapid high-resolution, multimode, fluorescence speckle microscopy and green fluorescent protein imaging in living cells, Methods Enzymol. 360 (2003) 597–617.
[27] E. Wang, C.M. Babbey, K.W. Dunn, Performance comparison between the high-speed Yokogawa spinning disc confocal system and single-point scanning confocal systems, J. Microsc. 218 (2005) 148–159.
[28] R.A. Hoebe, C.H. Van Oven, T.W. Gadella Jr., P.B. Dhonukshe, C.J. Van Noorden, E.M. Manders, Controlled light-exposure microscopy reduces photobleaching and phototoxicity in fluorescence live-cell imaging, Nat. Biotechnol. 25 (2007) 249–253.
[29] T. Wilson, A.R. Carlini, Size of the detector in confocal imaging systems, Opt. Lett. 12 (1987) 227–229.